Turkish Journal of Electrical Engineering & Computer Sciences

http://journals.tubitak.gov.tr/elektrik/

Research Article

Turk J Elec Eng & Comp Sci
(2018) 26: 1011 – 1026

doi:10.3906/elk-1706-287

# Simplification of harmonics filter for a matrix converter-based drive

**Gytis PETRAUSKAS[1,*], Gytis SVINKŪNAS[2], Rasa JURAŠKIENĖ[2]**
[1]Department of Automation, Faculty of Electrical and Electronics Engineering,
Kaunas University of Technology, Kaunas, Lithuania
[2]Department of Electric Power Systems, Faculty of Electrical and Electronics Engineering,
Kaunas University of Technology, Kaunas, Lithuania

**Received:** 23.06.2017 • **Accepted/Published Online:** 14.11.2017 • **Final Version:** 30.03.2018

**Abstract:** In this paper, an analysis of the interaction between the switching ripple filter components of a matrix converter-based drive and the components of a 0.4-kV electrical grid is presented. Based on the analysis, we propose a simplification of the conventional LCR filter. An inductance of the power grid transformer windings and an impedance of the power distribution lines could be considered as a filter component. Stemming from the above, a simplification of the filter topology is proposed. Only the capacitance component is necessary for realizing a conventional LCR filter. The effectiveness of this simplification is demonstrated through calculations, simulations performed in MATLAB/Simulink, and experimental results on a laboratory prototype.

**Key words:** Matrix converter, harmonics, filter

## 1. Introduction

The three-phase, purely semiconductor-based one-stage matrix converter (MC) is increasingly important in the industry, wind energy conversion systems, etc. [1–3]. Unlike two-stage diode supply-side inverters, MCs do not require an intermediate energy storage element. The lack of a bulky and relatively low-reliability DC link capacitor gives MCs inherent advantages that may be leveraged to improve size, cost, and reliability. The advancement of power semiconductor technologies will render MC-based drives a more attractive option over time [4,5].

The MC consists of nine bidirectional switches, whose output phases can all be connected to each of the three input phases, as shown in Figure 1. The bidirectional switches are commonly implemented using two diodes and two insulated-gate bipolar transistors (IGBTs). The MC, just like nonlinear loads such as thyristor bridges, arc furnaces, and cycloconverters, produces distorted harmonic currents into the electrical grid due to the discontinuous input currents, and voltage spikes are produced on the grid side [6]. Nowadays, power quality is important for electrical equipment and electrical energy consumers [7]. Passive filters comprise variable connection types for passive circuit elements; these filters have been used for many years, and are still used, because they remain economical [8]. Several papers have proposed topologies and methods for component value calculation of MC input filters. The input filter topology, principally proposed in the mentioned studies on MC application, is presented in Figure 2a. Since the MC can be considered a current source on the input side, an LCR circuit is usually adopted in the input filter with an attenuation resistor parallel to the inductor [9–16].

*Correspondence: gytis.petrauskas@ktu.lt

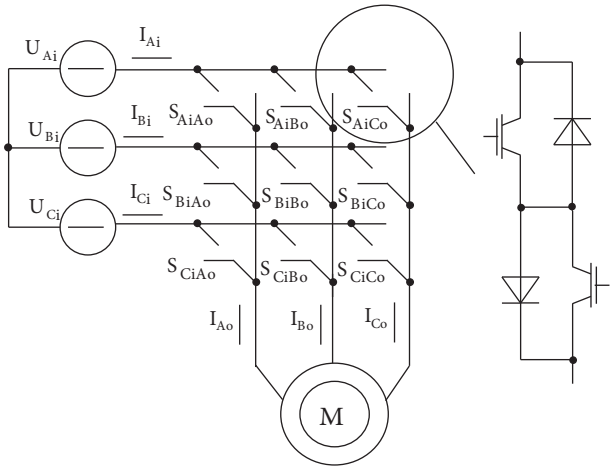


**Figure 1**. DMC-based drive power circuits.

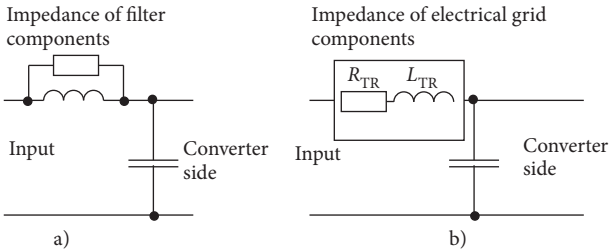


**Figure 2**. Components of MC input current.

There is almost no research on the unconventional topology of MC filters and filter parameter minimization. The LC resonant filter is mentioned in [17], but no detailed analysis is presented. A serial connection of two LC filters is proposed in [18], with the assertion that the attenuation rate of this connection is better compared to that of a single LC filter with the same power parameters. Methods for determining the LCR filter parameters are presented in [19], which offers to determine the value of filter inductance according to the voltage loss of the main harmonic and a filter attenuation rate of 26 dB, yet no detailed explanation is provided. The determination of the filter attenuation rate in accordance with the total current harmonic distortion rate of 5%, regulated by the IEEE 519 Standard, was proposed in [20], without considering that the impedance of the electrical grid components could influence the filter attenuation rate. The harmonics filtration problems of conventional converters with DC chain filters have been analyzed in [21]. This study proves that if the converter has significant power in comparison to the utility grid transformer, the application of filter inductivity hardly reduces the level of harmonics in the electricity network. These assumptions could be applied to harmonics attenuation in MC.

The calculation of the filter component value, considering the impedance of the electrical grid components, allows the application of a simplified filter topology, as presented in Figure 2b. The effectiveness of this simplified topology is demonstrated theoretically and by means of simulations and experiments.

The measurement and testing of supply voltage quality, according to EN 50160, require special measuring methods. The measured harmonic parameters are processed and recorded as 10-min time segments (1008 segments over 7 days). For each segment, the mean value of the measured parameter is calculated. After the 7-day recording period, a so-called ordered diagram is produced, which shows the sum of the duration of a given distortion level in the observed time period. The measured voltage harmonic parameters are maintained at the permissible level for 95% of the tested time. Therefore, the verification by MATLAB/Simulink and by experimental set was only performed by using induction motors fixed-state equivalent diagram.

According to this filter, simplification is expected to have a significant financial effect, making the MC viable for commercial proposition.

## 2. Topology and control of the researched MC

As presented in Figure 1, the MC is a forced commutated converter that uses an array of nine bidirectional switches as power elements to create a variable output voltage system with unrestricted frequency. It contains

no large energy storage elements. The key element of the MC is a fully controlled four-quadrant bidirectional switch that allows high-frequency operation. The 27 possible combinations (vectors) of bidirectional switches of a three-phase matrix converter can be realized. With an MC, the indirect space vector modulation (ISVM) can be applied to output voltage and input current control. In the ISVM, the desired output voltage and input current are synthesized from the active and zero vectors. As presented in Figure 3, the active and zero vectors are formed from 18 possible switch combinations (–9, –8 ... +8, +9). The active vectors have the following characteristics: two output lines are connected to a common input line, and the remaining output line is connected to another input line. Zero vectors have the following characteristic: all output lines are connected to a common input line.

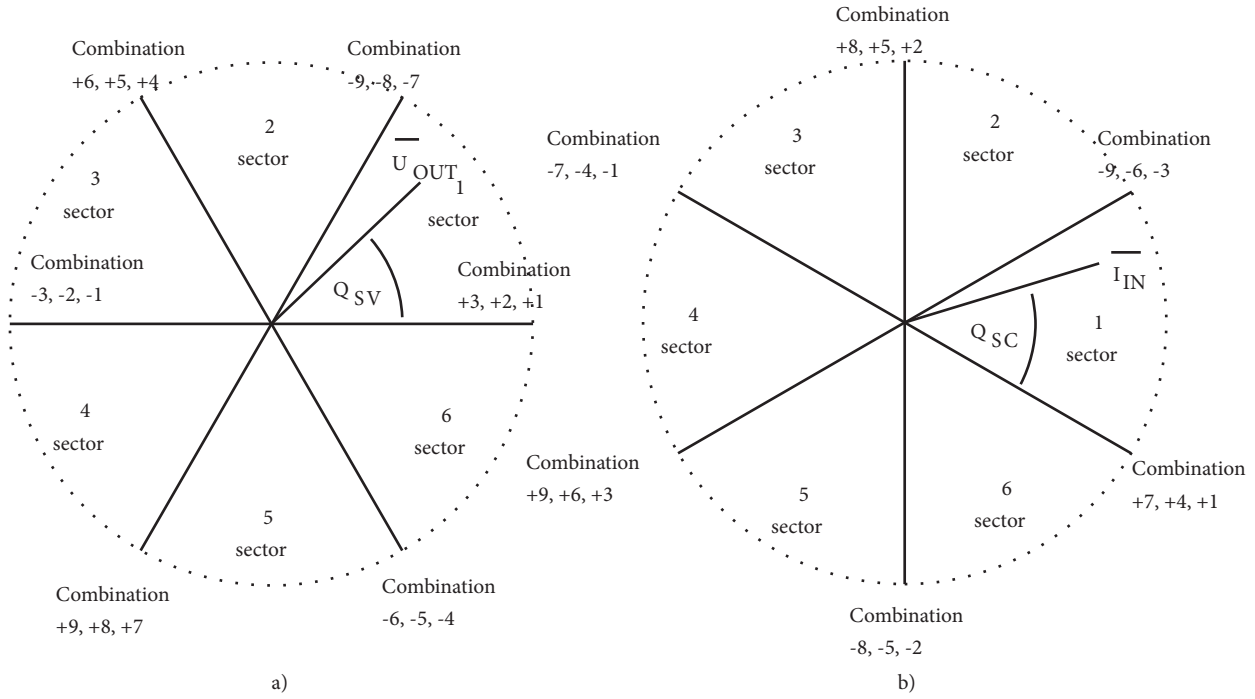


**Figure 3**. Single-phase equivalent diagram of three-phase input filters for the MC: a) conventional, b) simplified.

The space vector of the desired output line voltages and input currents are approximated by two adjacent, as shown in Figure 3.

The control algorithm of vector approximation is presented in Figure 4 [22]. According to the ISVM control strategy, it consists of two sequences, each representing the stages of rectifier and inverter. Each sequence consists of sector and duty cycle determination. Both sequences are combined by a common duty cycles determination segment and bidirectional switches control logic, as presented in Table 1.

## 3. Switching ripple harmonics generated by MC

The voltage of the switching ripples harmonic in the electrical grid can be determined based on the filter frequency response function:

$$U_{sw(n)} = H\left(j\omega\right) \times I_{sw(n)} \tag{1}$$

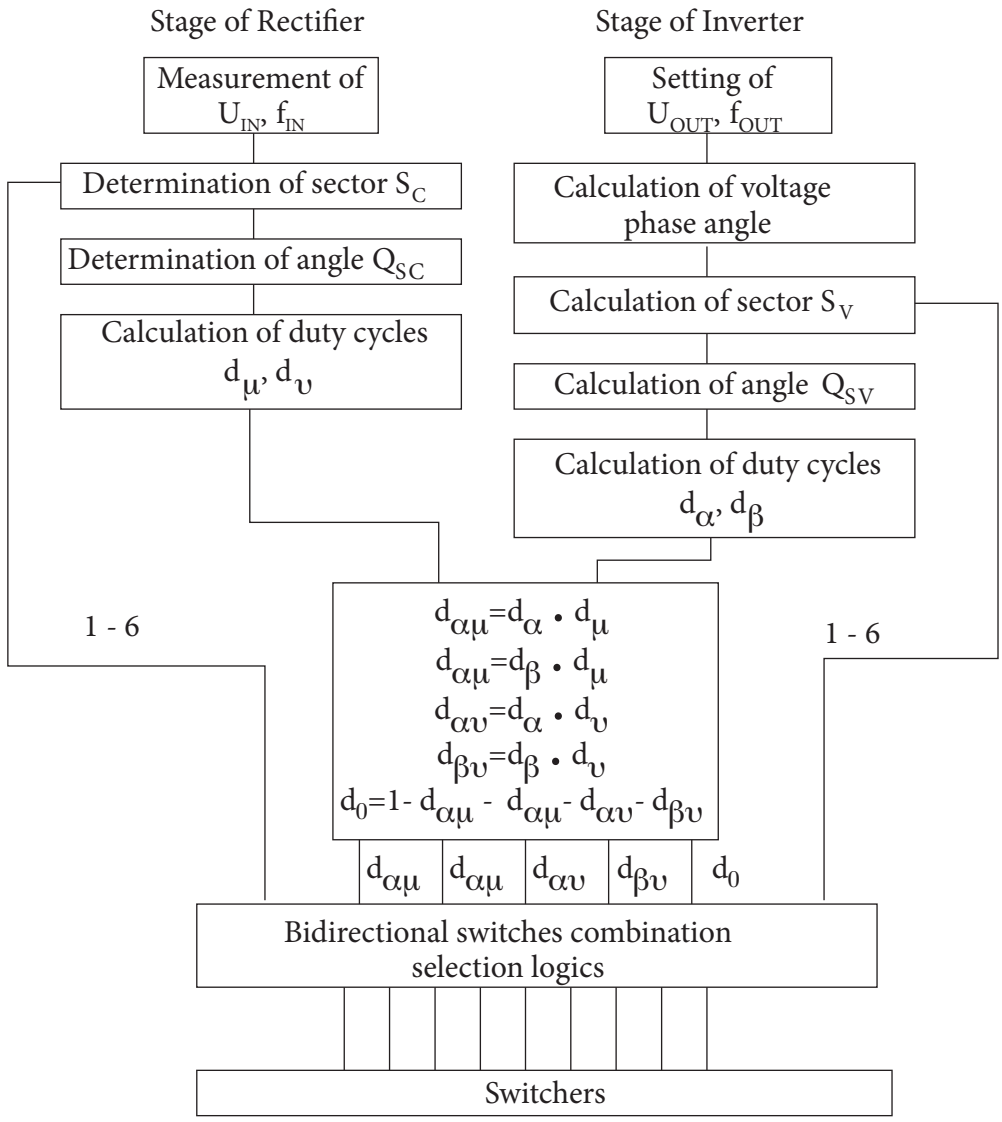


**Figure 4**. Graphical interpretation of a) sectors and direction of the output voltage vectors, b) sectors and directions of the input line current vectors.

where $I_{SW(n)}$ is the harmonic component of $I_{MC}$. The voltage level of the switching ripple harmonic in the utility grid should not exceed a few percent of the nominal voltage $U_{GRIDN}$. Practical research shows that increasing the 12-kHz harmonic voltage level to 10% of the $U_{GRIDN}$ causes damage to the electronic equipment after a few minutes [23]. A 12-kHz harmonic voltage level of 2%–3% of the $U_{GRIDN}$ causes no damage to the aforementioned equipment [23]. The maximum permitted level of harmonic voltage is 5%.

According to [24], the input current of MC is defined as

$$i_{Ai} = d_{\alpha\mu}(-i_{Bo}) + d_{\beta\mu}(i_{Ao}) + d_{\alpha\gamma}(-i_{Bo}) + d_{\beta\gamma}(i_{Ao}) \tag{2}$$

$$i_{Bi} = -d_{\alpha\mu}(-i_{Bo}) - d_{\beta\mu}(i_{Ao}) \tag{3}$$

**Table 1**. Bidirectional switches combination logic.

| | | Output voltage vector sectors $S_V$ | | | | | |
|---|---|---|---|---|---|---|---|
| | Sectors | 1 | 2 | 3 | 4 | 5 | 6 |
| Input current vector sectors $S_C$ | 1 | $-7+9+1-3$ | $+9-8-3+2$ | $-8+7+2-1$ | $+7-9-1+3$ | $-9+8+3-2$ | $+8-7-2+1$ |
| | 2 | $+4-6-7+9$ | $-6+5+9-8$ | $+5-4-8+7$ | $-4+6+7-9$ | $+6-5-9+8$ | $-5+4+8-7$ |
| | 3 | $-1+3+4-6$ | $+3-2-6+5$ | $-2+1+5-4$ | $+1-3-4+6$ | $-3+2+6-5$ | $+2-1-5+4$ |
| | 4 | $+7-9-1+3$ | $-9+8+3-2$ | $+8-7-2+1$ | $-7+9+1-3$ | $+9-2-3+2$ | $-8+7+2-1$ |
| | 5 | $-4+6+7-9$ | $+6-5-9+8$ | $-5+4+8-7$ | $+4-6-7+9$ | $-6+5+9-8$ | $+5-4-8+7$ |
| | 6 | $+1-3-4+6$ | $-3+2+6-5$ | $+2-1-5+4$ | $-1+3+4-5$ | $+3-2-6+5$ | $-2+1+5-4$ |
| Duty circles | | $d_{\alpha\mu}d_{\alpha v}d_{\alpha\mu}d_{\alpha v}$ | $d_{\alpha\mu}d_{\alpha v}d_{\alpha\mu}d_{\alpha v}$ | $d_{\alpha\mu}d_{\alpha v}d_{\alpha\mu}d_{\alpha v}$ | $d_{\alpha\mu}d_{\alpha v}d_{\alpha\mu}d_{\alpha v}$ | $d_{\alpha\mu}d_{\alpha v}d_{\alpha\mu}d_{\alpha v}$ | $d_{\alpha\mu}d_{\alpha v}d_{\alpha\mu}d_{\alpha v}$ |

$$i_{Ci} = -d_{\beta\mu}(i_{Ao}) - d_{\alpha\gamma}(-i_{Bo}) \tag{4}$$

where $i_{Ai}$, $i_{Bi}$,$i_{Ci}$ are input phase currents and $i_{Ao}$, $i_{Bo}$,$i_{Co}$ are output phase currents. During a fundamental frequency cycle, the maximal moment value of input current $i_{Ai}$ varies in time, and this time interval changes every 60°. The duty cycles presented in the equations change in the following order: $d_{\alpha\mu} \rightarrow d_{\beta\mu} \rightarrow d_{\beta\gamma} \rightarrow d_{\alpha\gamma}$ . Using the law of sines, the duty cycles can be written as in [24]:

$$d_{\alpha\mu} = \sin(60^\circ - \theta_{SW}) \ \ \sin(60^\circ - \theta_{SC}) \tag{5}$$

$$d_{\beta\mu} = \sin\theta_{SW} \cdot \sin(60^\circ - \theta_{SC}) \tag{6}$$

$$d_{\beta\gamma} = \sin\theta_{SW} \cdot \sin\theta_{SC} \tag{7}$$

$$d_{\alpha\gamma} = \sin(60^\circ - \theta_{SW}) \cdot \sin\theta_{SC} \tag{8}$$

where $\theta_{SW}$ and $\theta_{SC}$ are the angles between input and output current. The angles change in intervals 0–60° with different angular speeds. The angular speeds depend on input and output current frequency, and various combinations of $\theta_{SW}$ and $\theta_{SC}$ are possible. The curves of input currents in duty cycles are presented in Figure 5.

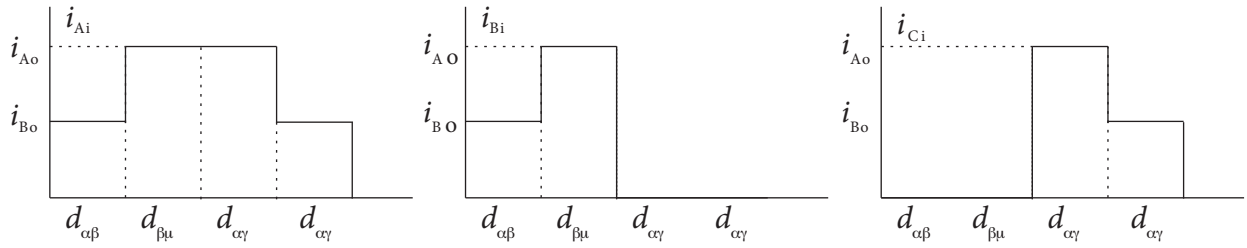


**Figure 5**. Graphical interpretation of switcher's combination selection algorithm.

A harmonics spectrum of input current depends on its relationship with input currents $i_{Ai}$ and $i_{Bi}$ in the time interval. The maximum potential difference between these currents in case of $i_{Ai} = 1$ and $i_{Bi} = -0.86$. The harmonics spectrum for phase A input current could be described by the Fourier line:

$$i_{Ai}(t) = I_{SW0} + I_{SW1}\sin(\omega_{SW1}t + \varphi_1) + I_{SW2}\sin(2\omega_{SW2}t + \varphi_2) + I_{SWn}\sin(n\omega_{SWn}t + \varphi_n) \tag{9}$$

$$\omega_{SW} = 2\pi f_{SW} \tag{10}$$

$$I_{SW0} = i_{Bo}\left(d_{\alpha\mu} + d_{\alpha\gamma}\right) + i_{Ao}\left(d_{\beta\mu} + d_{\beta\gamma}\right) \tag{11}$$

$$I_{SWn} = \sqrt{I_{SWn}{'2} + I_{SWn}^{''2}} \tag{12}$$

$$\varphi_n = arctg\left(\frac{I_{SWn}^{''2}}{I_{SWn}^{'2}}\right) \tag{13}$$

where $n$ is number of harmonics.

The components of the Fourier line for phase A current are as follows:

$$I'_{SWn} = -\frac{i_{Bo}}{n\pi}\left(\cos(nd_{\alpha1}2\pi) - 1\right) + \frac{i_{Ao}}{n\pi}\left(\cos(nd_{\alpha3}2\pi) - \cos(nd_{\alpha1}2\pi)\right) - \frac{i_{Bo}}{n\pi}\left(\cos(nd_{\alpha4}2\pi) - \cos\left(nd_{\alpha3}2\pi\right)\right) \tag{14}$$

$$I"_{SWn} = \frac{i_{Bo}}{n\pi}\left(\sin(nd_{\alpha1}2\pi) - sin0^{\circ}\right) + \frac{i_{Ao}}{n\pi}\left(\sin(nd_{\alpha3}2\pi) - \sin(nd_{\alpha1}2\pi)\right) + \frac{i_{Bo}}{n\pi}\left(\sin\left(nd_{\alpha4}2\pi\right) - \sin\left(nd_{\alpha3}2\pi\right)\right) \tag{15}$$

where $d_{\alpha1} = d_{\alpha\mu}$, $d_{\alpha3} = d_{\alpha\mu} + d_{\beta\mu} + d_{\beta\gamma}$, $d_{\alpha4} = d_{\alpha\mu} + d_{\beta\mu} + d_{\beta\gamma} + d_{\alpha\gamma}$.

The components of the Fourier line for phase B and C currents are as follows:

$$I'_{SWn} = -\frac{i_{Bo}}{n\pi}\left(\cos(nd_{\alpha\mu}2\pi) - cos0^{\circ}\right) - \frac{i_{Ao}}{n\pi}\left(\cos\left(n(d_{\alpha\mu}+d_{\beta\mu}\right)2\pi\right) - \cos(nd_{\alpha\mu}2\pi)), \tag{16}$$

$$I"_{SWn} = \frac{i_{Bo}}{n\pi}\left(\sin(nd_{\alpha\mu}2\pi) - sin0^{\circ}\right) + \frac{i_{Ao}}{n\pi}\left(\sin(n(d_{\alpha\mu}+d_{\beta\mu})2\pi\right) - \sin(nd_{\alpha\mu}2\pi)). \tag{17}$$

The level of switching components $K_{HAR} = I_{SW1}/I_{SW0}$ in the input current of MC for current phase of maximal moment value (during special time interval of maximal phase A), presented in Figures 6a and 6b, is relatively low and varies in the range of 10%–50%. Such ripple content is for 1/3 of a time interval. The level of switching components $K_{HAR}$ in the input current of the MC for current phases of minimal moment values (during a special time interval of minimal phase B and C) is quite different. The level of switching components $K_{HAR} = I_{SW1}/I_{SW0}$ for minimal moment value phases, presented in Figures 6c and 6d, is relatively high and varies in the range of 40%–200%. Such content of ripples is for a time interval of 2/3 of a period. An average harmonic content of $I_{SW1}$ in the input current is approximately 100% of the total harmonics content. The calculation of filter component values must be based on this assumption. According to the IEEE 519 Standard, the level of switching components should not exceed 5%. Therefore, the average attenuation of the switching ripple filter has to be 26 dB ($20lg\frac{100}{5}$) for the time interval of maximal currents, and 32 dB ($20lg\frac{200}{5}$) for the time interval of minimal currents. The filter of this attenuation level would not allow the level of switching ripple harmonics to exceed 5%.

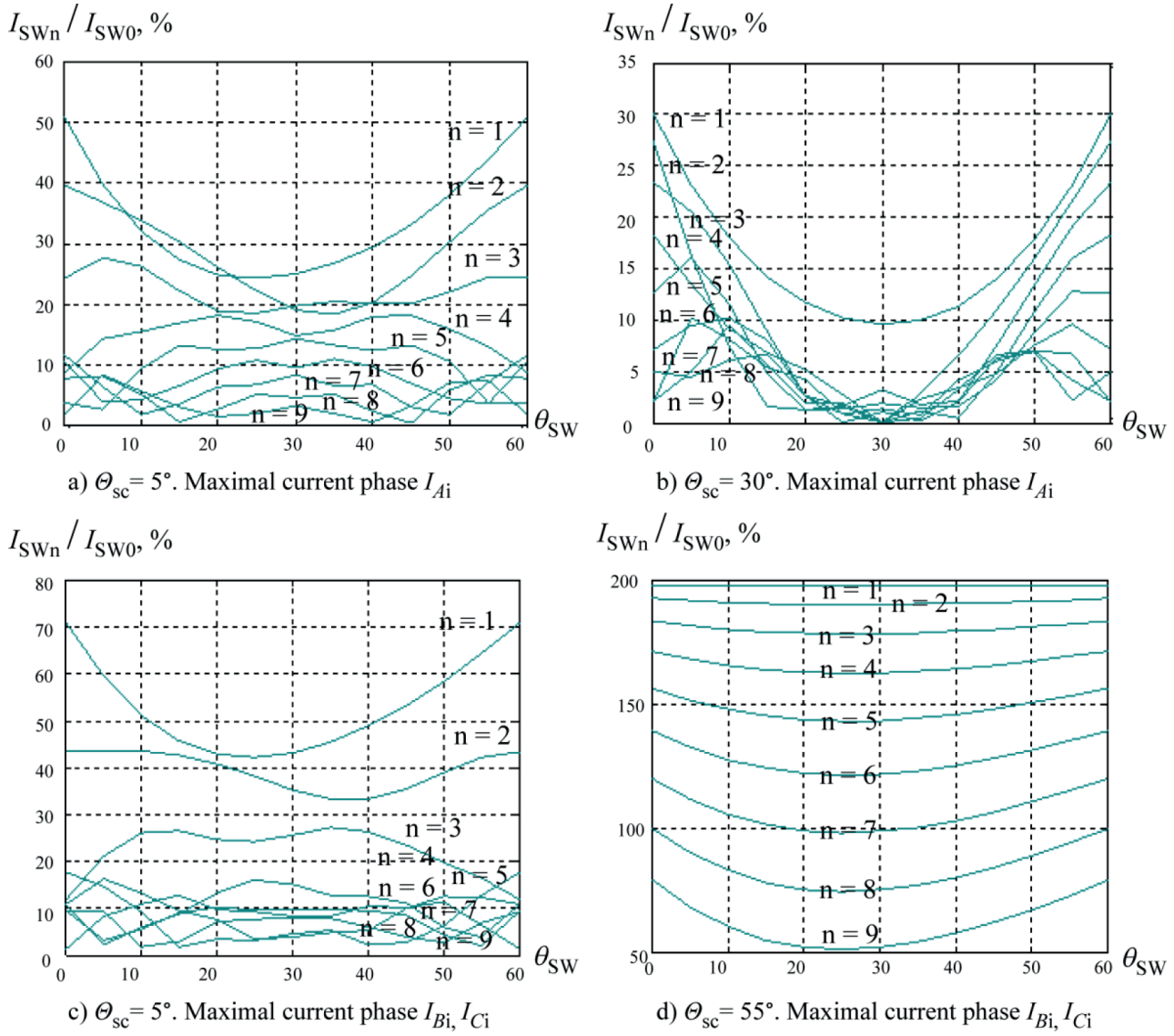


**Figure 6**. Switching ripple harmonics components.

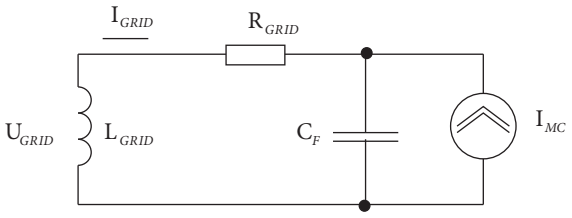


**Figure 7**. Single-line diagram of simplified filter.

## 4. Calculation of conventional LCR filter component values

A single-phase equivalent diagram system electrical grid (LCR filter) matrix converter is presented in Figure 7. The determination of the filter voltage response $H_U$ is based on MC input side conductivity:

$$B_F = \frac{1}{\frac{1}{j\omega C_F}} + \frac{1}{j\omega(L_F + L_{GRID})} = j\omega C_F - j\frac{1}{\omega\,(L_F + L_{GRID})} = j\left(\omega C_F - \frac{1}{\omega\,(L_F + L_{GRID})}\right)$$
$$= j\frac{\omega^2 C_F\,(L_F + L_{GRID}) - 1}{\omega\,(L_F + L_{GRID})} \tag{18}$$

$$H_U\,(j\omega) = \frac{U_{GRID}}{I_{MC}} = \frac{I_{MGRID}\,j\,\omega\,L_{GRID}}{I_{MC}} \tag{19}$$

$$I_{GRID} = \frac{I_{MC}\ \frac{1}{j\omega\,(L_F + L_{GRID})}}{B_F} = \frac{I_{MC}}{I_{MC}\ \times\ j\omega(L_F + L_{GRID})} \tag{20}$$

$$H_U\,(j\omega) = \frac{\frac{I_{MC}\times j\omega L_{GRID}}{B_F\times j\omega(L_F + L_{GRID})}}{I_{MC}} = \frac{(L_{GRID})}{B_F\ \times\ (L_F + L_{GRID})} = j\frac{\omega\,(L_F + L_{GRID})}{\omega^2 C_F\,(L_F + L_{GRID}) - 1} \times \frac{(L_{GRID})}{(L_F + L_{GRID})}$$
$$= -j\frac{\omega\,(L_{GRID})}{\omega^2 C_F\,(L_F + L_{GRID})\ -\ 1} \tag{21}$$

$$H_U\,(j\omega) = \frac{U_{GRID}}{I_{MC}} = -j\frac{\omega\,(L_{GRID})}{\omega^2 C_F\,(L_F + L_{GRID}) - 1} \tag{22}$$

where $L_{GRID}$ is the induction value of the grid transformer and the power distribution line; $L_F$ is the induction value of the filter; $C_F$ is the capacitance of the filter; and $U_{GRID}$ is the line-to-line voltage of the power distribution line.

The determination of the filter current response $H_I$ is as follows:

$$H_I\,(j\omega) = \frac{H_U(j\omega)}{j\omega\,(L_{GRID})} = \frac{1}{\omega^2 C_F\,(L_F + L_{GRID}) - 1} \tag{23}$$

This is in case of

$$\omega^2 C_F L_F \gg 1, \tag{24}$$

$$H_I\,(j\omega) = \frac{1}{\omega^2 C_F\,(L_F + L_{GRID})} \tag{25}$$

The calculation filter component values usually begin from the capacitance value, based on the consideration that $Q_{CF} = K_C S_{MC}$. The proposed value $K_C$ =0.1.

$$C_F = \frac{K_C\,S_{MC}}{j3U_{GRID}^2\omega_{GRID}} \tag{26}$$

The calculation of the filter inductance value is based on the consideration that the voltage drop $K_L$ in the LCR filter inductance is approximately 5% of the grid voltage. The proposed value of $K_L$ =0.05.

According to this consideration,

$$\sqrt{3}\,I_{MC}\,\omega\,L_F = K_L\,U_{GRID} \tag{27}$$

$$I_{MC} = \frac{S_{MC}}{\sqrt{3}\,U_{GRID}} \tag{28}$$

$$L_F = \frac{K_L\, U_{GRID}^2}{S_{MC}\, \omega_{GRID}} \tag{29}$$

$$L_{GRID} = \frac{0.05\, U_{GRID}^2}{S_{GRID}\, \omega_{GRID}} \tag{30}$$

Substituting $L_F$ for $C_F$ in Eq. (25), the filter current response can be written as

$$H_I\,(j\omega) = \frac{3}{\left(\frac{\omega}{\omega_{GRID}}\right)^2 K_L\, K_C} \tag{31}$$

According to Eq. (31), the filter attenuation rate can be calculated on the basis of the voltage drop and the reactive power of the filter components.

## 5. Level of switching ripple harmonics generated by the MC

The level of harmonics can be calculated on the basis of the $H_I(j)$ value and evaluated according to the IEEE 519 Standard. The level of harmonics depends on the relative load between the MC power and the power of the electrical grid $S_{MC}\,/\,S_{GRID}$. According to standard EN 50160, it has not exceeded 1.5%–2%.

The components of switching ripple harmonics are as follows:

$$K_{SW} = \frac{U_{SW1}}{U_{GRID}} = \frac{\sqrt{3} I_{SW} \omega_{SW} L_{GRID}}{U_{GRID}} \tag{32}$$

$$I_{SW} = \frac{I_{MC} K_{HAR}}{H_I} = \frac{S_{MC} K_{HAR}}{\sqrt{3} U_{GRID} H_I} \tag{33}$$

where $K_{HAR} = \frac{I_{SW1}}{I_{SW0}}$. The value $K_{HAR} = 0.5$ is accepted according to the level of switching components presented in Figure 6a.

Substituting $I_{SW}$ Eq. (33) and $L_{GRID}$ Eq. (30) in Eq. (32),

$$K_{SW} = \frac{S_{MC}\, \omega_{SW}\, 0.05\, K_{HAR}}{S_{GRID}\, \omega_{GRID}\, H_I} \tag{34}$$

In the case of high-power MC in comparison to the power of the grid transformer, the $K_{SW}$ is relatively high. When $\frac{S_{MC}}{S_{GRID}} = \frac{1}{4}$ , $\frac{\omega_{SW}}{\omega_{GRID}} = \frac{8000}{50} = 160$, $H_I = 20$, $K_{HAR}$= 0.5, $K_{SW} = 0.05$ or 5%. The voltage of the switching ripples harmonic $U_{SW}$ is sufficiently high. Because of this, the 26-dB attenuation of switching ripple harmonics by LCR filter is sufficient only in the case of relatively low-power MC. For the high-power MC, the attenuation of the filter has to be verified according to Eq. (34).

## 6. Calculation of simplified filter component values

Due to filter simplification by using grid transformer and distribution line inductance $L_{GRID}$ as filter components, the frequency response $H\,(\mathrm{j}\omega)$ of an inductanceless filter ($L_F = 0$, $C_{F1}$) has to be identified and compared to the response of a conventional filter:

$$H\,(j\omega) = -j\frac{\omega\,(L_{GRID})}{\omega^2 C_F\,(L_F + L_{GRID}) - 1} = -j\frac{\omega\,(L_{GRID})}{\omega^2 C_{F1}\,(L_{GRID}) - 1} \tag{35}$$

The same attenuation rate of the filter is

$$\omega^2 C_F \left(L_F + L_{GRID}\right) = \omega^2 C_{F1} \left(L_{GRID}\right) \tag{36}$$

$$C_{F1} = C_F \frac{L_F + L_{GRID}}{L_{GRID}} \tag{37}$$

Substituting the above-presented in Eqs. (21) and (22):

$$C_{F1} = C_F \left(1 + \frac{S_{GRID}}{S_{MC}}\right) \tag{38}$$

According to Eq. (35), to achieve the necessary attenuation rate of an inductanceless filter, the capacitance value has to be increased. In the case of $S_{GRID}/S_{MC} = 1$, the value of filter capacitance $C_{F1}$ has to be doubled; in the case of $S_{GRID}/S_{MC} = 2$, the value of filter capacitance $C_{F1}$ has to be tripled, and so on. This means that the application of an inductanceless filter is possible only in the case of a high-power MC-based drive. However, in the case of $S_{GRID}/S_{MC} = 3$ and $Q_{CF1} = 0.3\ S_{MC}$, the value of the phase angle between the voltage and the current of the MC input will be high enough ($\varphi = 21.8°$), and further increments are not recommended. Therefore, the application of an inductanceless filter is recommended in the case of an MC-based drive power $S_{MC} > 0.35\ S_{GRID}$.

Figure 8 presents the frequency responses $H(j\omega)$ of conventional ir inductanceless filters in the case of a 100-kVA grid transformer loaded with a 50-kW MC-based drive. It is noted that there is not much difference among them, and the efficacy of the inductanceless filter will not be lower.

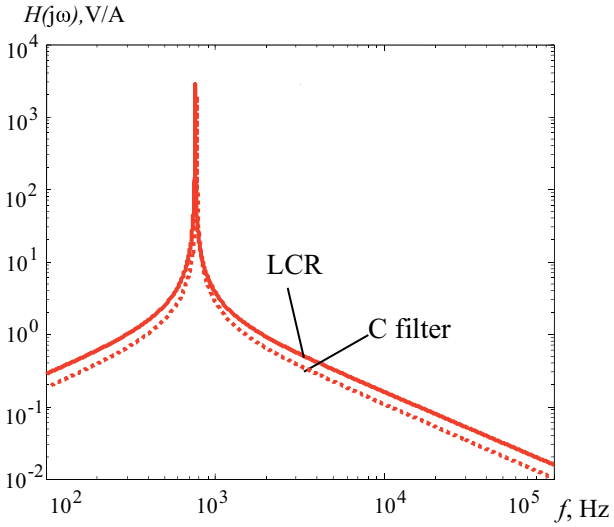


**Figure 8**. Frequency response of the LCR and C filters, derived in MATLAB/Simulink, in the case of a 100-kVA grid transformer loaded with a 50-kW MC-based drive.

In order to prevent a resonant in filter circuits, the attenuation resistance has to be connected in parallel to filter inductivity, as presented in Figure 2a. The value of the attenuation resistance depends on the attenuation rate [19].

$$Q_{PAR} = R_D \sqrt{\frac{C_F}{L_F}} = 3 \div 5. \tag{39}$$

In the case of filter simplification, the inductivity of power transformer winding is used instead of the additional inductivity component. Only active serial resistance of transformer winding, as presented in Figure 2b, prevents the resonant. The attenuation quality rate of the serial contour can be calculated as follows:

$$Q_{SER} = \frac{1}{R_{TR}}\sqrt{\frac{L_{TR}}{C_F}} = \frac{\omega_R L_{TR}}{R_{TR}} \tag{40}$$

Comparing the quality of parallel and serial attenuation:

$$\frac{1}{R_{TR}}\sqrt{\frac{L_{TR}}{C_F}} = R_D\sqrt{\frac{C_F}{L_F}} \tag{41}$$

The value of attenuation resistance can be easily determined:

$$R_D = \frac{1}{R_{TR}}\left(\frac{L_F}{C_F}\right) \tag{42}$$

Following the above equations, the sufficiency of transformer windings active resistance is determined and presented in Table 2. It can be seen that the active resistance of transformer windings is insufficient for resonant attenuation. Consequently, the elimination of resonant attenuation resistor is applicable only in the case of sufficient internal active resistance power distribution lines.

**Table 2**. Values of power transformer and filter components.

| | 40 kVA | 1000 kVA |
|---|---|---|
| $R_{TR}$ | 90 mΩ | 1.7 mΩ |
| $X_{TR}$ | 156 mΩ | 8.6 mΩ |
| $S_{MC}$ | 10 kW | 250 kW |
| $C_{F1}$ | 18 $\mu$F | 450 $\mu$F |
| $Q_{SER}$ | 28 | 72 |
| Estimation | Resonant | Resonant |

## 7. Verification

In order to verify the theoretical results obtained in the previous sections, the filter discussed above was tested using a computer simulation and experimented on using a laboratory prototype. The simulation was developed in MATLAB/Simulink. The MATLAB/Simulink model of the researched system consists of four parts. The first part contains the electrical grid components simulation blocks—impedance of a 10/0.4 kV transformer, power distribution lines, and a connection cable. As presented in Figure 9a the MATLAB/Simulink blocks implementing three-phase series RLC branch were used. The second part contains blocks for filter component simulation. As presented in Figure 9b, MATLAB/Simulink blocks were used, implementing ideal sinusoidal AC voltage source and three-phase series RLC branch. The third part contains nine ideal bidirectional switches of the MC and ISVM control modules. As presented in Figure 10, for nine bidirectional switches, MATLAB/Simulink blocks implementing an IGBT device and a diode in parallel with a series RC snubber circuit were used. For the ISVM controls, presented in Section 2, we used two subsystems in MATLAB/Simulink. The subsystems comprise input and output modulators. In modulators we used the MATLAB/Simulink blocks implementing the following:

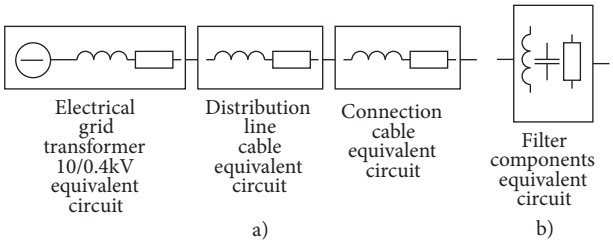


**Figure 9**. Structure of a) electrical grid components simulation model, b) filter components simulation model.

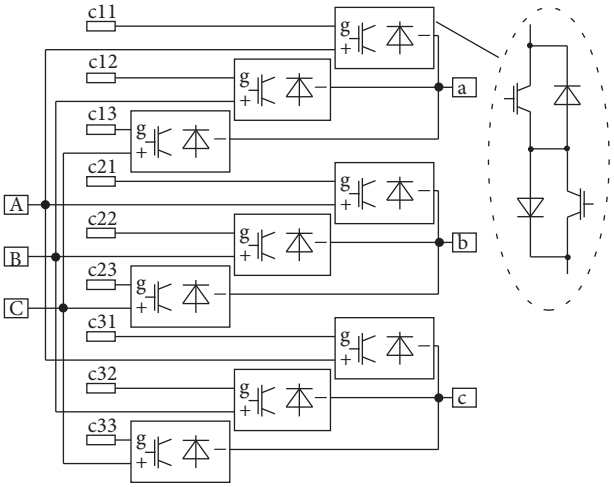


**Figure 10**. Structure of a nine ideal bidirectional switches simulation model.

- Three-phase system transformation into two alpha and beta vectors;
- Alpha and beta vector transformation into degree and magnitude vectors;
- Logical operators for vector sector determination;
- Duty cycle determination and switching pattern definition blocs.

The fourth part contains an MC load, which is presented as an equivalent diagram of the induction motor [25]. As presented in Figure 11, MATLAB/Simulink blocks, implementing three-phase series RL branch, were used.

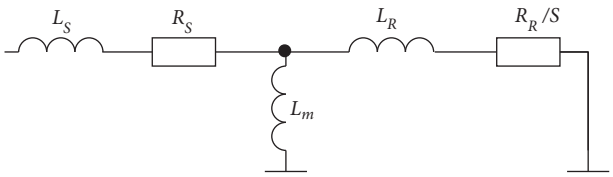


**Figure 11**. Single-line diagram of induction motor equivalent circuit.

The matrix drive caused harmonic distortion in the power distribution lines damped by conventional LCR. Simplified C filters are presented as a function of relative load $S_{MC}/S_{GRID}$ in Figure 12a. The simulation results show that the application of a simplified C-based filter allows one to keep the voltage distortion level within the range permitted by the IEEE 519 Standard. The filter component value calculation, including grid component impedance as a filter design, allows reducing the current distortion level in the power distribution lines.

According to a study of the influence of operating frequency on induction motor equivalent circuits, presented in [25], the equivalent resistance Reqsc increases by 45%, with an increase in the frequency of input voltage from 50 Hz to 300 Hz. The corresponding Reqsc values were assigned in MATLAB/Simulink.

According to the ISVM strategy, presented in Section 2, the control system virtually divides the MC into the stages of rectifier and inverter. The frequency of MC output voltage and the speed of the induction machine depend on inverter stage. The harmonic content of input voltage and the power factor of the MC converter depend on the rectifier stage. Because of this virtual division, the frequency variations on the inverter stage

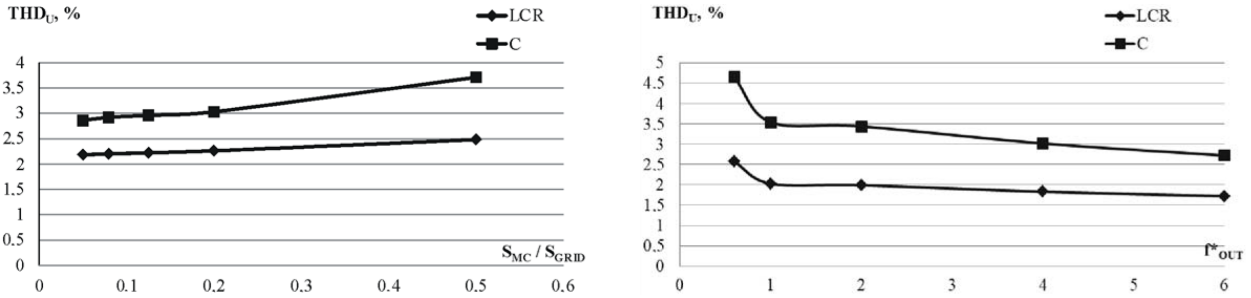


**Figure 12**. Total harmonic distortion of matrix drive input voltage $U_{MC}$ as a function of a) relative load of a grid transformer with constant output voltage frequency; b) relative frequency of MC output voltage.

of the MC should not affect the efficiency of the MC input filter in switching ripple harmonics damping. Only an increase in equivalent resistance Reqsc could affect the harmonics level. Figure 12b presents the level of voltage harmonic distortion at the interconnection point of the MC and electrical grid distribution lines as a function of MC inverter stage operation relative frequency $f_{MC}/f_{GRID}$, maintaining a constant value of input current RMS. The diagram shows that the level of voltage harmonic distortion at the MC and distribution line connection point does not increase the permitted values in the standards by increasing the frequency.

Experimental validation was carried out on a 0.5-kW MC laboratory prototype using IGBT-based, four-quadrant switches commutated under an 8-kHz switching frequency. The experiment was carried out in reduced supply voltage $U_{GRID} = 110$ V. As presented in Figures 13 and 14, the laboratory prototype consists of several components, listed below:

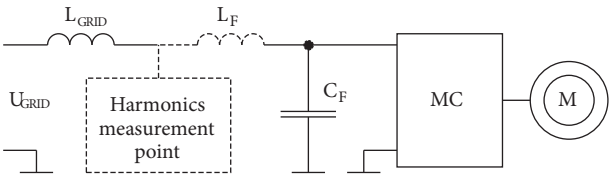


**Figure 13**. Single-line diagram of the experimental setup.

- electrical grid impedance imitation components;
- filter components;
- MC with space vector modulation controller;
- motor equivalent circuit.

The experiment was carried out in reduced supply voltage $U_{GRID} = 110$ V. An $L_{GRID} = 1$ mH inductor was connected for the imitation of high-power electrical grid component impedance. An equivalent circuit of a 33 Ω active resistor and a 3-mH inductor for the inductor motor windings imitation were connected to the MC output. The load power of the MC laboratory prototype is equal to 25% of the power of the grid transformer. The LCR filter of $L_F = 4$ mH and $C_F = 4$ μF at the input of the MC was calculated according to Eqs. (26) and (29), and connected for ripple harmonics attenuation. This is for the case of $K_L = 0.03$, $K_C = 0.1$, and a filter attenuation of 26 dB, as shown in Eq. (31). The aforementioned values of the filter components must ensure the necessary distortion attenuation.

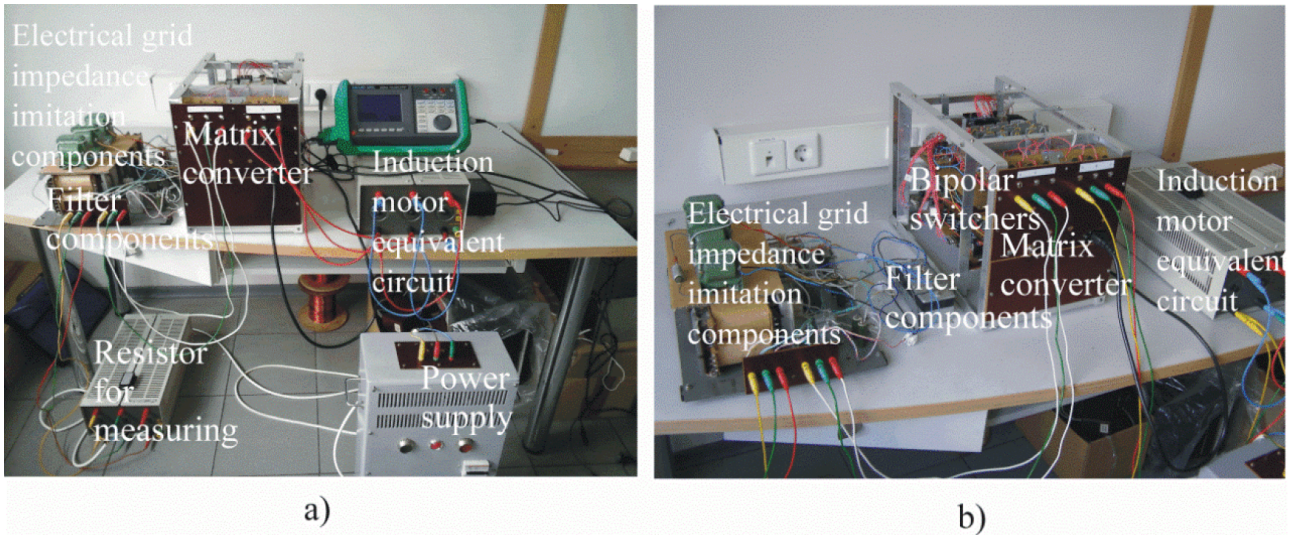


**Figure 14**. Configuration of the experimental setup: a) LCR filter, b) C-filter.

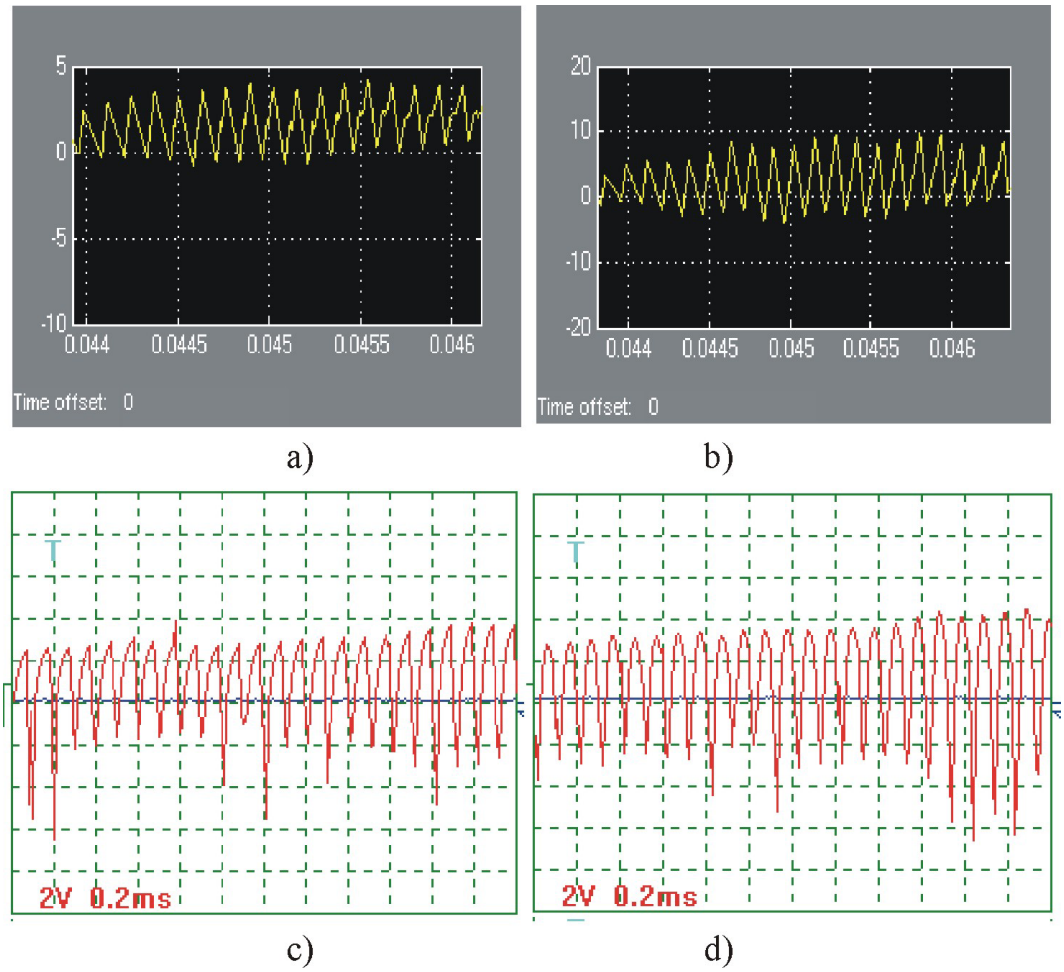


**Figure 15**. Fragment of the voltage sin wave in MC-based drive loaded power distribution line, taken from: a) MATLAB/Simulink LCR filter, b) MATLAB/Simulink C filter, c) experimental setup LCR filter-eliminating grid frequency, d) experimental setup C filter-eliminating grid frequency.

As shown in Figure 15a, the level of the ripple frequency harmonics in the case of an LCR filter is approximately 3 V, which is 2.7% of the supply voltage. The experimental results coincide with the results of the MATLAB/Simulink simulation. Figure 15b shows the level of the ripple frequency harmonics using the simplified C filter topology (value of filter component $C_F = 16\ \mu$F). This is approximately 4.5 V, which is 3.5% of the supply voltage. The harmonics voltage measured in the experiment is lower in comparison to the values calculated by Eq. (34) due to the higher $K_{HAR}$ value. Additionally, it coincides with the MATLAB/Simulink simulation results showing an insignificant increase in the voltage distortion level. It can be stated that the C filter ensures the permissible by EN50610 standard distortion levels in the power distribution lines in the case of a high-power, MC-based induction motor drive.

## 8. Conclusion

The reviewed studies on matrix converter ripple harmonics attenuation do not assess the impedance of an electrical grid 10/0.4 kV transformer, power distribution lines, and connection cable in the filter components value calculation. By performing harmonics spectrum analysis, the formula-relating level of harmonics, grid impedance, and filter attenuation rate are derived. The mentioned formula is substantial in the case of high-power MC. Considering the impedance of grid components, only capacitance is indispensable for conventional MC input filter realization, keeping harmonic distortion within the level permitted by the standard. According to this study, the application of an inductanceless filter is possible only in the case of a high-power MC-based drive. The application of an inductanceless filter is recommended for MC-based drive power $S_{MC} > 0.35\ S_{GRID.}$ It is especially applicable to wind energy conversion systems with MC-based double-fed induction generators that have significantly high relative power $S_{MC} / S_{GRID}$.

## References

[1] Coşkun I, Saygın A. Speed control of induction motor by matrix converter. Gazi University Journal of Science 2004; 17: 63-76.

[2] Bharanikumar R, Kumar A. Performance analysis of wind turbine-driven permanent magnet generator with matrix converter. Turk J Elec Eng & Comp Sci 2012; 20: 299-317.

[3] Potamianos PG, Kappatou J, Safacas AN, Mitronikas ED, Michalatos P. Modeling of a matrix converter fed induction machine drive system for diagnostic purposes. Int T Elec Energy Syst 2015; 25: 405-418.

[4] Safari S, Castellazzi A, Wheeler P. Experimental and analytical performance evaluation of SiC power devices in the matrix converter. IEEE T Power Electr 2014; 29: 2584-2596.

[5] Salem T, Wood R. 1000-H evaluation of a 1200-V, 880-A all-SiC dual module. IEEE T Power Electr 2014; 29: 2192-2198.

[6] Kocatepe C, Kekezoğlu B, Bozkurt A, Yumurtacı R, İnan A, Arıkan O, Baysal M, Akkaya Y. Survey of power quality in Turkish national transmission network. Turk J Elec Eng & Comp Sci 2013; 21: 1880-1892.

[7] Jashfar S, Esmaeili S, Zareian-Jahromi M, Rahmanian M. Classification of power quality disturbances using S-transform and TT-transform based on the artificial neural network. Turk J Elec Eng & Comp Sci 2013; 21: 1528-1538.

[8] Rustemli S, Cengiz MS. Active filter solutions in energy systems. Turk J Elec Eng & Comp Sci 2015; 23: 1587-1607.

[9] Wang X, Lin H, Feng B, Lyu Y. Damping of input LC filter resonance based on virtual resistor for matrix converter. In: 2012 IEEE Energy Conversion Congress and Exposition; 15–20 September 2012; Raleigh, NC, USA. New York, NY, USA: IEEE. pp. 3910-3916.

[10] Szczesniak P, Urbanski K, Fedyczak Z, Zawirski K. Comparative study of drive systems using vector-controlled PMSM fed by a matrix converter and a conventional frequency converter. Turk J Elec Eng & Comp Sci 2016; 24: 1516-1531.

[11] She H, Lin H, Wang X, Yue L. Damped input filter design of matrix converter. In: IEEE 2009 International Conference on Power Electronics and Drive Systems; 2–5 November 2009; Taipei, Taiwan. New York, NY, USA: IEEE. pp. 672-677.

[12] Erdem E, Tatar Y, Sünter S. Effects of input filter on stability of matrix converter using Venturini modulation algorithm. In: IEEE 2010 International Symposium on Power Electronics Electrical Drives Automation and Motion; 14–16 June 2010; Pisa, Italy. New York, NY, USA: IEEE. pp. 1344-1349.

[13] Karaca H, Akkaya R. Control of Venturini method based matrix converter in input voltage variations. In: IAENG 2009 International MultiConference of Engineers and Computer Scientists; 18–20 March 2009; Hong Kong, Hong Kong. Hong Kong, Hong Kong: IAENG. pp. 1412-1416.

[14] Wang J, Bouazdia M. Influence of filter parameters/topologies on stability of matrix converter-fed permanent magnet brushless motor drive systems. In: IEEE 2009 Electric Machines and Drives Conference; 3–6 May 2009; Miami, FL, USA. New York, NY, USA: IEEE. pp. 964-970.

[15] Ragusa A, Zanchetta P, Empringham L, De Lillo L, Degano M. High frequency modelling method of EMI filters for hybrid Si-SiC matrix converters in aerospace applications. In: IEEE 2013 Applied Power Electronics Conference and Exposition; 17–21 March 2013; Long Beach, CA, USA. New York, NY, USA: IEEE. pp. 2610-2617.

[16] Rivera M, Rojas C, Rodrıguez J, Wheeler P, Wu B, Espinoza J. Predictive current control with input filter resonance mitigation for a direct matrix converter. IEEE T Power Electr 2011; 26: 2794-2803.

[17] Wheeler P, Grant D. Optimized input filter design and low-loss switching techniques for a practical matrix converter. IEE P-Elect Pow Appl 1997; 144: 53-60.

[18] Trentin A, Zanchetta P, Clare J, Wheeler P. Automated optimal design of input filters for direct AC/AC matrix converters. IEEE T Ind Electron 2012; 59: 2811-2823.

[19] Dasgupta A, Sensarma P. An integrated filter and controller design for direct matrix converter. In: 2011 IEEE Energy Conversion Congress and Exposition; 17–22 September 2011; Phoenix, AZ, USA. New York, NY, USA: IEEE. pp. 814-821.

[20] Safari S, Castellazzi A, Wheeler P. The impact of switching frequency on input filter design for high power density matrix converter. In: 2014 IEEE Energy Conversion Congress and Exposition;14–18 September 2014; Pittsburgh, PA, USA. New York, NY, USA: IEEE. pp. 579-585.

[21] Svinkunas G, Medvedev K. Simulation of frequency converters operation in industrial power net. Electron Elec Eng 2012; 1: 65-70.

[22] Petrauskas G, Svinkunas G. Modified control of the matrix converter based drive for voltage sag impact reduction. Turk J Elec Eng & Comp Sci 2017; 25: 2243-2260.

[23] Svinkunas G. Power quality standard and voltage quality problems in Lithuanian distribution network. In: IEEE 2005 Power Tech Russia; 27–30 June 2005; St. Petersburg, Russia. New York, NY, USA: IEEE. pp. 1-5.

[24] Huber L, Borojevic D. Space vector modulated three-phase to three-phase matrix converter with input power factor correction. IEEE T Ind Appl 1995; 31: 1234-1246.

[25] De Martin M, Bailoni M, Tessarolo A, Bortolozzi M, Giulivo D, Agnolet F, Santarossa R. Investigation into induction motor equivalent circuit parameter dependency on current and frequency variations. In: 2014 International Conference on Electrical Machines; 2–5 September 2014; Berlin, Germany. New York, NY, USA IEEE. pp. 196-202.